A Global Thermal Conductivity Model for Lunar Regolith at Low Temperatures. A. Martinez[1,2] and M. A. Siegler[1,2], J. M. Martinez-Camacho[1,2], [1]Planetary Science Institute (1700 East Fort Lowell, Suite 106 Tucson, AZ 85719-2395, angelicamtz@smu.edu), [2]Southern Methodist University, Dallas, TX.

Introduction: Although some of the coldest surface temperatures in the entire Solar System are found near the poles of our own Moon, the thermophysical properties of lunar regolith at these low temperatures (i.e., below ~150 K) are not well understood. Standard lunar thermal models [e.g., 1,2] are generally in good agreement with surface temperatures observed by lunar remote sensing data but are inconsistent with data collected from permanently shadowed regions (PSRs). PSRs are primary areas of interest for lunar exploration due to their incredibly cold temperatures (<100 K), which provide a favorable thermal environment for the cold trapping of water ice and other organic volatiles. Our ability to predict the stability of such volatiles is, in part, dependent on the constraints we have on the thermal properties of lunar materials at these low temperatures.

We present an updated thermal conductivity model for lunar regolith that produces a previously unaccounted for drop in thermal conductivity at low temperatures. Thermal model results produce larger (when compared to standard thermal models) diurnal temperature amplitudes typically observed in PSRs [3]. Because of the reduced thermal conductivity at low temperatures, an additional result of this model is the ability to predict warmer average subsurface temperatures, up to 15 K warmer at 2-meter depths in modeled PSRs (Shoemaker crater). This may have significant implications for the cold trapping of volatiles such as water ice, carbon dioxide, and sulfur dioxide.

Data Set: The one-dimensional thermal models used to test the thermal conductivity model are compared with derived brightness temperature data collected by the Diviner Lunar Radiometer Experiment (Diviner) onboard the Lunar Reconnaissance Orbiter (LRO). We use the Global Cumulative Products (GCP) accessible through the Planetary Data System (PDS) to acquire a gridded data set with a 2-pixel-per-degree spatial resolution (~15 km) and 0.25 h local time resolution [4]. We compare diurnal surface temperatures produced by our thermal models with relatively flat and rock-free regions of the lunar surface by excluding Diviner data with more than 1% rock abundance and slopes greater than 1º [5,6]. Diviner channel 7 (*T7*, 25 – 41mm) is used to represent a physical surface temperature due to its high signal-to-noise ratio and insensitivity to small and hot rocks [2,7]. We derive thermal conductivity model parameters that best fit preliminary laboratory data found in [8]. This laboratory data consists of thermal conductivity measurements of NU-LHT-2M lunar simulant for the temperature range of 15 K to 205 K at a single bulk density of ~1,700 kg/m^3.

Approach and Methods: The effective thermal conductivity of lunar regolith may be represented as the summation of a temperature-independent solid conduction term, k_c, and a temperature-dependent radiative term, k_r,

$$k_{eff} = k_c + k_r \quad (1)$$

where k_c is proportional to a constant A and k_r is proportional to the cube of temperature *T*. We adopt the approach carried out by [9] and apply a temperature dependence (amorphous endmember) to the solid conduction term, k_c. We derive a general density and temperature-dependent model to describe the effective thermal conductivity:

$$k_{eff}(T,\rho) = A(\rho)k_{am}(T) + B(\rho)T^3 \quad (2)$$

Here, $k_{am}(T)$ is the temperature-dependent solid conduction component taken from equation (30) in [9]. We apply nonlinear fits using equation (2) to scaled laboratory measurements from [8] to derive the form and coefficients of the density-dependent terms $A(\rho)$ and $B(\rho)$. Since our goal is to create a model that works globally (i.e., both at warm low latitudes and cooler high latitudes), scaling the lab data to coincide with the thermal conductivity profile in the standard model [1] will provide us with a basic preliminary model that we can then modify as needed to match Diviner data. The final form of the effective thermal conductivity is expressed in equation (3) (in SI units W m^{-1} K^{-1}). Profile

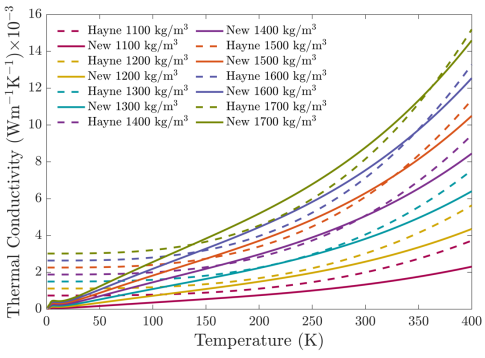

Figure 1. Thermal conductivity profile comparison between the standard model [1] and an updated model using equation (3) as the thermal conductivity.

comparisons between the standard and new thermal conductivity models are illustrated in Figure 1.

$$k_{eff}(T,\rho) = (A_1\rho - A_2)k_{am}(T) + (B_1\rho - B_2)T^3 \quad (3)$$

$$A_1 = 5.0821 \times 10^{-6}$$
$$A_2 = 5.1 \times 10^{-3}$$
$$B_1 = 2.0022 \times 10^{-13}$$
$$B_2 = 1.953 \times 10^{-10}$$

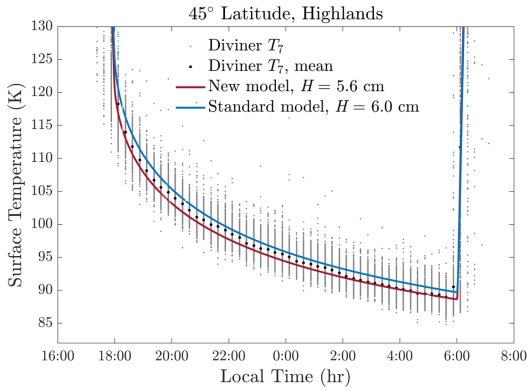

Figure 2. Nighttime curve comparison at 45º highlands latitude. The two model results are compared with average temperature readings from Diviner. This location incorporates Diviner data at 45 ± 25º latitude.

Results: The new thermal conductivity model produces similar diurnal surface temperatures in warmer, low latitude regions, though slightly cooler nighttime surface temperatures are observed (e.g., Figure 2). Average subsurface temperatures increase with latitude. By 80º latitude, the difference reaches approximately 8 K in the highlands about ~6 K in the mare at 60º latitude [e.g., Figure 7 in 10]. Because the new thermal conductivity model deviates most significantly from the previous model below ~150 K, we find the most notable outcome of the new model is the sharp increase in subsurface thermal gradients for shadowed near-polar craters. Thermal model results for a PSR located in Shoemaker crater (Figure 3) show a slight increase in diurnal surface temperature amplitudes. Figure 4, however, shows that the reduced thermal conductivity at low temperatures produces a steeper geothermal gradient and shallower depth of penetrating thermal wave. A 4-meter depth temperature map of Shoemaker crater in Figure 5 indicates that the new thermal conductivity model may produce up to a 30 K increase in mean temperature. Such drastic increase in temperature at depth has important implications for the long-term stability and behavior of trapped volatiles in lunar polar terrain.

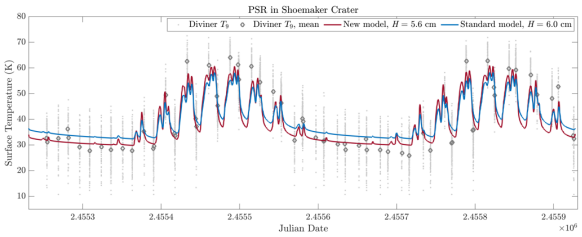

Figure 3. Surface temperature calculations of a PSR in Shoemaker crater compared with average Diviner channel 9 observations. The selected site is located at 87.9102º S and 45.5073º E.

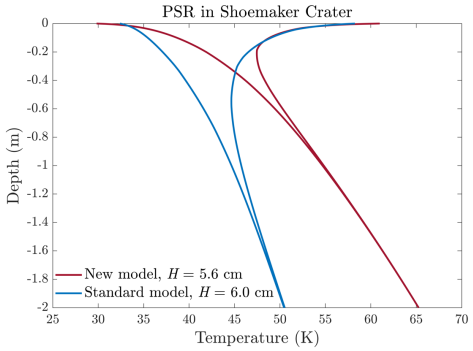

Figure 4. Subsurface temperature profile comparison of the standard model [1] and the new model for a PSR located within Shoemaker crater.

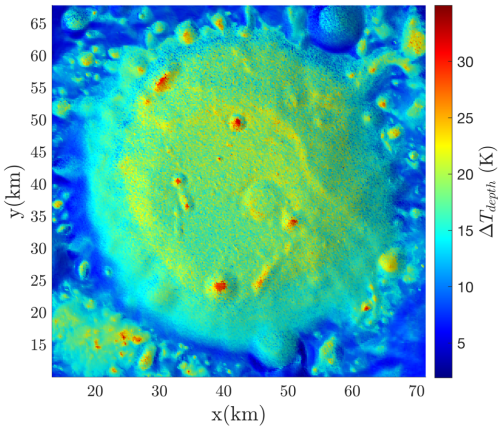

Figure 5. Mean temperature difference (between standard and new model) map of Shoemaker crater at 4-meters depth.

References: [1] Hayne et al. (2017) *JGR, 122*(12), 2371-2400. [2] Vasavada et al. (1999) *Icarus, 141*(2), 179-193. [3] Paige et al. (2010) *Science*, *330*(6003), 479–482. [4] Paige, D. (2020), NASA Planetary Data System. [5] Paige, D. (2017), NASA Planetary Data System. [6] Lucey et al. (2014) *JGR, 119*(7), 1665–1679. [7] Feng et al. (2020) *JGR,* 125, e2019JE006130. [8] Zhong et al. (2016) *LPSC,* (p. 2995). [9] Woods-Robinson et al. (2019) *JGR, 124*(7), 1989–2011. [10] Martinez A. and Siegler M. A. (2021) *JGR*, *126,* e2021JE006829